Oxidation of silicon nitride hot pressed with Y_2O_3 + MgO

G. N. BABINI, A. BELLOSI, P. VINCENZINI
C.N.R., Research Institute for Ceramics Technology, Faenza, Italy

Oxidation tests of silicon nitride hot pressed with combined Y_2O_3 and MgO additions in the compatibility field Si_3N_4–Si_2N_2O–$Y_2Si_2O_7$, performed at 1193 to 1658 K under 98 kPa air atmosphere for 30 h, result in parabolic oxidation kinetics and three different oxidation regimes. At $T < \sim 1400$ ($\Delta H = 120\ kJ\ mol^{-1}$) oxygen diffusion is suggested to be the more probable limiting step for oxidation, whereas at higher temperatures, diffusion of additive and impurities appears rate-controlling ($\Delta H = 580\ kJ\ mol^{-1}$). The very high oxidation rates and ΔH values ($\Delta H = 960\ kJ\ mol^{-1}$) at $T > 1600$ K are possibly associated with a softening of the grain-boundary phase. The existance of silicate solid solutions in the grain-boundary phase which are able to accomodate additive and impurity cations in their structure might explain the very good oxidation resistance of (Y_2O_3 + MgO)-doped HPSN at $T < 1400$ K.

1. Introduction

The superior high-temperature mechanical strength and oxidation resistance of some yttria-doped hot-pressed silicon nitride (HPSN) materials derive from their very high refractory and partially or totally crystalline grain-boundary phase formed during hot pressing or reheating. Only compositions of the compatibility field Si_3N_4–Si_2N_2O–$Y_2Si_2O_7$ of the Si_3N_4–Y_2O_3–SiO_2 system in which the occurrence of the four quaternary compounds $Y_{10}Si_7O_{23}N_4$ (H-phase), $YSiO_2N$ (K-phase), $Y_4Si_2O_7N_2$ (J-phase) and $Si_3Y_2O_3N_4$ is avoided, show good oxidation resistance at all temperatures [1, 2].

Materials containing one or more of such phases, which all oxidize linearly and catastrophically [1–3] prove unsuitable for use at intermediate temperatures, i.e. ~ 1273 K, due to their degradation under oxidizing conditions. Other experimental evidence [4–6] suggests that compositions belonging to the compatibility triangle Si_3N_4–$Y_2Si_2O_7$–H-phase can also offer a good oxidation resistance, provided that among the quaternary compounds only the H-phase is present and in limited amounts.

Owing to the high refractoriness of the grain-boundary phase, Y_2O_3-doped silicon nitride requires high hot-pressing temperatues and shows difficulty in being pressureless sintered to high density. Al_2O_3 [7] and MgO [8] have been used in combination with Y_2O_3 to obtain high dense materials using normal sintering. Sialons are generally formed when using Al_2O_3, whereas the combined use of MgO and Y_2O_3 allows high densities to be reached by reaction sintering without affecting the intrinsic structure of the nitride phase.

The present study was aimed to analyse the oxidation behaviour of a fully dense hot-pressed material obtained from a composition of the Si_3N_4–Y_2O_3–MgO system, which proved particularly suited to obtain silicon nitride compacts by pressureless sintering. The results, therefore, can be assumed to be an indication of the best oxidation resistance characteristics one may expect for these materials.

2. Materials and methods

The oxidation tests were performed on a hot-pressed fully converted > 99% dense (3.20 g cm^{-3}) material containing reagent grade 8 wt% Y_2O_3 and 1 wt% MgO as the densification aid, i.e. belonging to the low oxidation field of the ternary Si_3N_4–SiO_2–Y_2O_3. This composition

0022–2461/83/010231–14$04.18/0 © *1983 Chapman and Hall Ltd.*

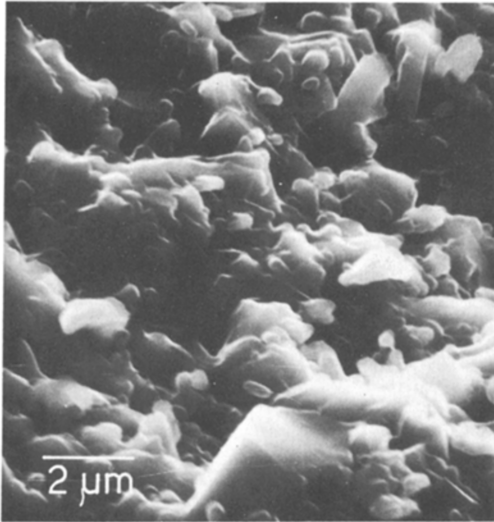

Figure 1 Scanning electron micrograph of a fracture surface of (8 wt% Y_2O_3 + 1 wt% MgO)-doped silicon nitride hot pressed at 1973 K and 350 kg cm^{-2} for 30 min.

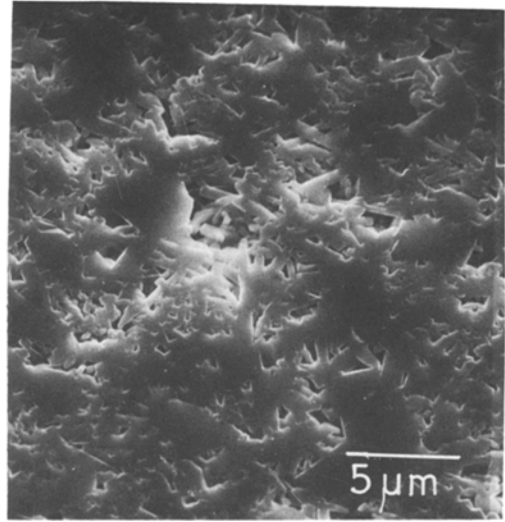

Figure 2 SEM of a polished and etched surface of the sample of Fig. 1.

was pressureless sintered up to 96 to 97 relative density [8]. Preparation steps included wet milling of the additive to 0.5 to 2 μm, mixing and homogenizing the silicon nitride powder* with the additive in isobutyl alcohol for 72 h in a plastic jar and alumina ball mills, drying, screening and hot pressing at 1973 K and 34.3 MPa for 30 min in a BN-lined graphite die. Microstructural observations performed by X-ray diffraction (XRD)†, SEM‡, and wavelength dispersive spectroscopy (WDS)§ analysis suggest that during hot pressing, an intergranular liquid phase is formed by reaction of surface silica and silicon nitride grains with the additive. Part of the intergranular phase crystallizes to the yttrium silicates miserite (Ca, K, Na, Al, Y) · SiO_3 [9] and z-$Y_2Si_2O_7$ [10] (see Table I). By further heat treatments in air of the hot-pressed samples, crystallization of the grain-boundary phase increases: limited amounts of silicon oxynitride (possibly deriving from the oxidation of β-Si_3N_4) form at $T \geqslant 1473$ K. α- and δ-$Y_2Si_2O_7$ [11, 12] were detected after heat treatments up to 1658 K whereas z-$Y_2Si_2O_7$ disappeared. Both miserite and yttrialite ((H, Ne, Fe)$Y_5Si_6O_{21}$) [13], stable at intermediate temperature, decompose upon heating at $T \geqslant 1400$ K.

SEM observations performed on fractures (Fig. 1) and polished and etched (molten NaOH, 5 sec, Fig. 2) surfaces reveal some non-homogeneous distribution of the intergranular phase. Small β-Si_3N_4 grains are locally embedded in the second phase whereas the width of the boundary between Si_3N_4 grains in some instances is so small as not to be evidenced by SEM observations. The grain size also spreads over a broad spectrum (0.2 to 6 μm). A SEM back-scattered electron image (Fig. 3) shows the topology of phase distribution: black areas indicate residual pores, grey areas the silicon nitride grains and the white areas the intergranular phase enriched in additive and impurity atoms.

The square samples (10 mm × 10 mm × 2 mm), used for the oxidation tests were diamond-cut from the hot-pressed billet, wet-polished with various grades of diamond paste up to 1 μm, and ultrasonically cleaned in acetone. The oxidation experiments were carried out in 98 kPa air atmosphere. Weight gain was continuously recorded by using a TG apparatus¶ capable of 2×10^{-5} g

*AME-Refractory Grade. BET specific surface area 3.72 m^2 g^{-1}; amorphous SiO_2 1.9 wt%; Si (metal) 1.4 wt%; chemical analysis: Si (total) 58.41%; N 37.73%; Al 0.42%; Fe 0.46%; Ca 0.13%, Mg 220 ppm; Na 120 ppm; K < 50 ppm; α/β ratio 3.8 (volumetric). Grain size (determined by TEM) 150 nm.
†Siemens D 500.
‡Etec Autoscan.
§Etec Austospec.
¶Netzsch Geratebau.

TABLE IA Semiquantitative evaluation of crystalline phase observed on outer surface of oxidized samples

Oxidation temperature* (K)	Crystalline phase content†											
	β-Si_3N_4	Miserite (Ca, K, Na, Al, Y) · SiO_2	z-$Y_2Si_2O_7$	Yttrialite (H, Na, Fe) $Y_5 \cdot Si_6O_{21}$	Cristobalite SiO_2	Akermanite $MgO \cdot 2CaO \cdot 2SiO_2$	Diopside $CaO \cdot MgO \cdot SiO_2$	$Y_2O_3 \cdot 2SiO_2$	$Y_2Si_2O_7$	Protoenstatite $MgSiO_3$	Enstatite + clinoenstatite $MgSiO_3$	Quartz SiO_2
Unoxidized	90	8	2	–	–	–	–	–	–	–	–	–
1193	72	6	4	4	7	7	traces	–	–	–	–	–
1283	75	5	traces	5	5	7	3	–	–	–	–	–
1383	60	4	–	4	16	7	5	2	–	–	–	–
1403	59	4	–	4	14	9	6	4	–	–	–	–
1493	36	–	–	–	15	traces	traces	6	2	34↗	7	–
1593	7	–	–	–	7	–	–	19↗	4	17↗	46	–
1658	traces	–	–	–	22	–	–	20↗	traces	–	40	18

TABLE IB Semiquantitative evaluation of crystalline phase observed in their bulk

	β-Si_3N_4	Miserite	Yttrialite	Si_2N_2O	α-$Y_2Si_2O_7$	δ-$Y_2Si_2O_7$
1193	70	7	4	–	12	7
1493	64	7	3	4	14	8
1658	59	3	–	20	11	7

*Soak time 30 h in air.

†Numbers refer to the heights of selected XRD peaks normalized to 1.

↗Oriented phase.

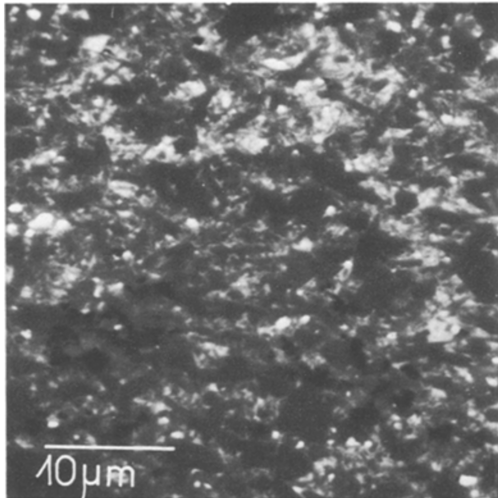

Figure 3 SEM back-scattered electron image of the sample in Fig. 1 (black areas: residual pores; grey areas: β-Si_3N_4; white areas: grain-boundary phase).

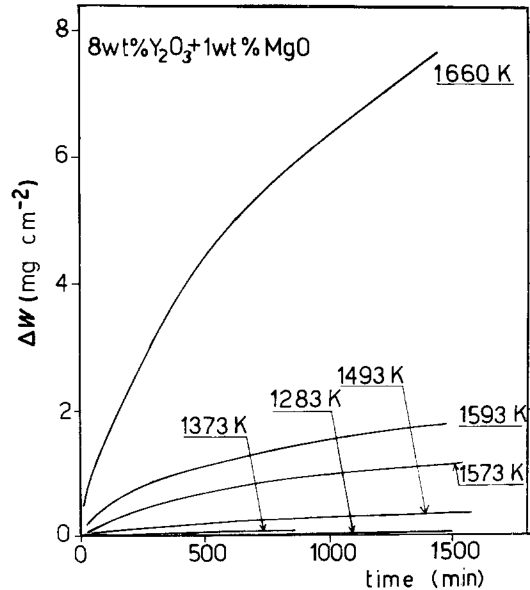

Figure 4 Parabolic plots for oxidation in air of hot-pressed Si_3N_4 doped with 8 wt% Y_2O_3 + 1 wt% MgO.

resolution. Oxidation temperatures ranged from 1193 to 1658 K; the heating and cooling rates were 20 and 10 K min^{-1}, respectively. A constant oxidation time of 30 h was generally used but more prolonged (100 h) oxidation experiments were also performed in order to compare different additive systems. Before and after oxidation, the samples were weighed to $\pm 1 \times 10^{-5}$ g.

Surfaces and cross-sections of the oxide scales were analysed by XRD, SEM, including back-scattered electron imaging, and WDS.

3. Results

3.1. Oxidation kinetics

The plots of weight gain against time for the 8 wt% Y_2O_3 + 1 wt% MgO material oxidized in air at 1193 to 1658 K approximate the classical parabolic behaviour which can be represented by the equation:

$$W^2 = K \cdot t + C_0 \sim K \cdot t$$

where $K = K_0 \exp(-\Delta H/RT)$ (mg cm^{-2} min^{-1}) is the parabolic oxidation rate constant, W is the weight gain at time t and C_0 is a constant that adjusts for the small initial nonparabolic behaviour which derives in part from the uncertainty of the time zero. In the present case C_0 appears negligible. No detectable weight gain occurred during tests at < 1083 K.

Plots of the squares of the weight gain as a function of time are shown in Fig. 4. The parabolic rate constants, K, determined from the slopes of

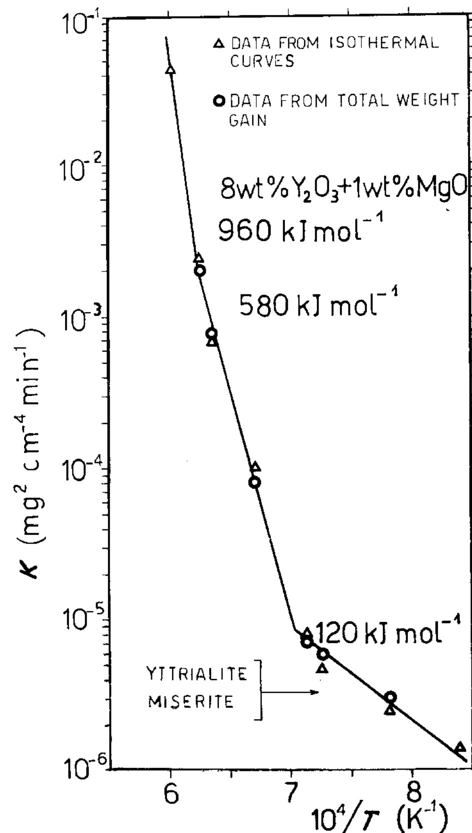

Figure 5 Arrhenius plot of oxidation rate constants derived from Fig. 4 for hot-pressed Si_3N_4 doped with 8 wt% Y_2O_3 + 1 wt% MgO.

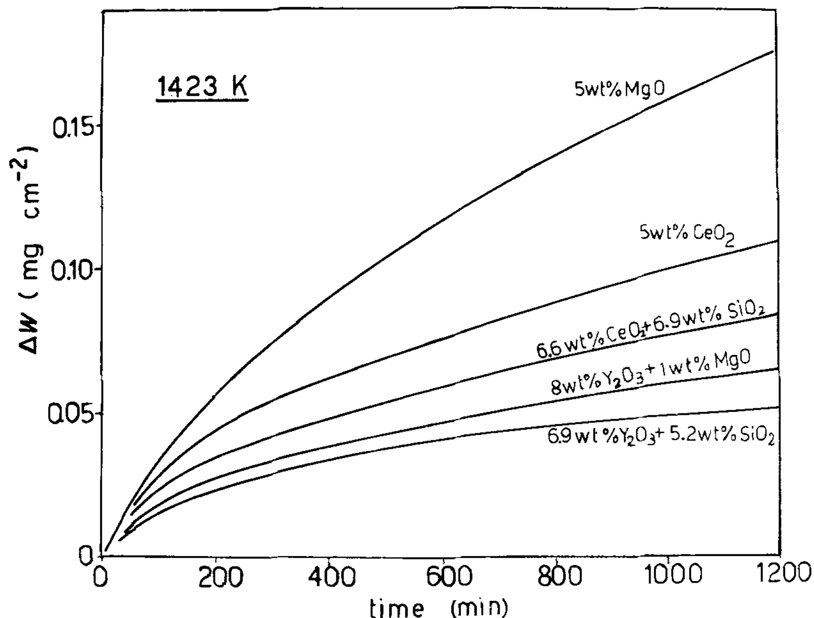

Figure 6 Isothermal weight gain curves in air at $T = 1423$ K for hot-pressed Si_3N_4 doped with different sintering aids.

the straight lines of Fig. 4 and reported as a function of temperature in the Arrhenius plot of Fig. 5, give three different values for the activation energy for different temperature regions, i.e. $120\,kJ\,mol^{-1}$ at $\leqslant 1423$ K, $580\,kJ\,mol^{-1}$ at $1423 < T < 1623$ K and $960\,kJ\,mol^{-1}$ at $\geqslant 1623$ K. The open circles in Fig. 5 denote the results of the oxidation rate constants calculated from the weight gains determined by weighing the samples before and after the oxidation run and assuming parabolic kinetics.

Figs 6 and 7 show the results of long-term oxidation tests (100 h) at $T = 1423$ and 1573 K for materials prepared with the same Si_3N_4 powder

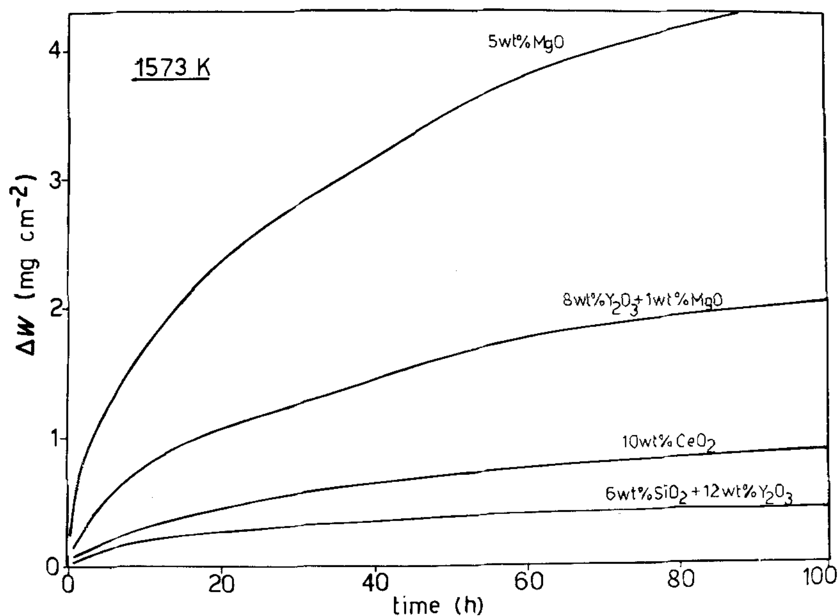

Figure 7 Isothermal weight gain curves for oxidation in air at $T = 1573$ K for hot-pressed silicon nitride doped with different sintering aids.

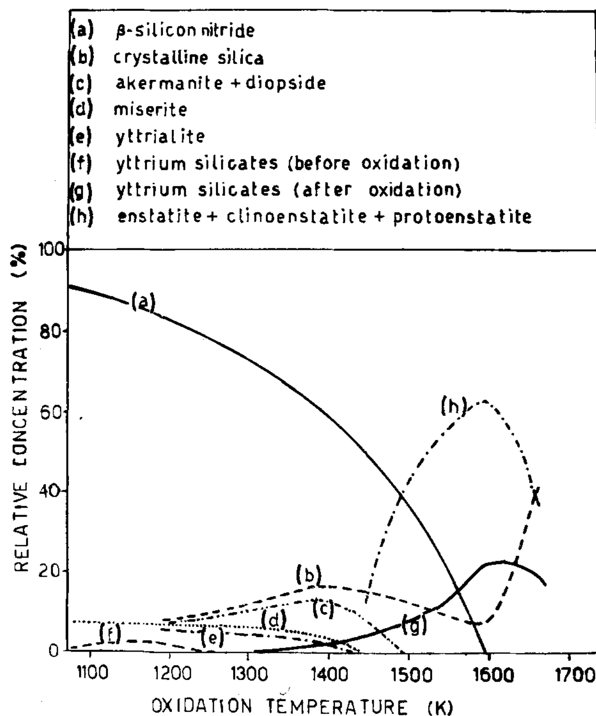

Figure 8 Semiquantitative contents of crystalline phases present on the outer surfaces for hot-pressed Si_3N_4 doped with 8 wt% Y_2O_3 + 1 wt% MgO oxidized at various temperatures for 30 h.

and containing different sintering aids.* At $T =$ 1423 K the 8 wt% Y_2O_3 + 1 wt% MgO composition appears superior to all other additive systems except the yttria–silica material, whereas at $T =$ 1573 it approximates the behaviour of the MgO compositions which show the worst oxidation behaviour.

3.2. Characterization of the oxide scales

Fig. 8 shows the relative amounts of crystal phases present on the oxide-layer surface as a function of the oxidation temperature, obtained by room-temperature semi-quantiative XRD analysis. SEM micrographs, including back-scattered electron images and WDS maps of the surface and cross-section morphology of the oxide films formed after 30 h oxidation at various temperatures, are shown in Figs 9 to 17.

By combining kinetics and microstructural data it is possible to account for the different oxidation behaviour associated with the three different temperature regions of Fig. 5.

3.2.1. Oxidation at temperatures up to 1440 K

At < 1440 K yttrialite and miserite are stable crystal forms; only the excess Ca, Mg and other impurity metallic ions which cannot be accomodated in the lattice of the above crystal phases should possibly be involved in the oxidation. At low temperature, i.e. below 1283 K, oxidation effects appear preferentially located at concen-

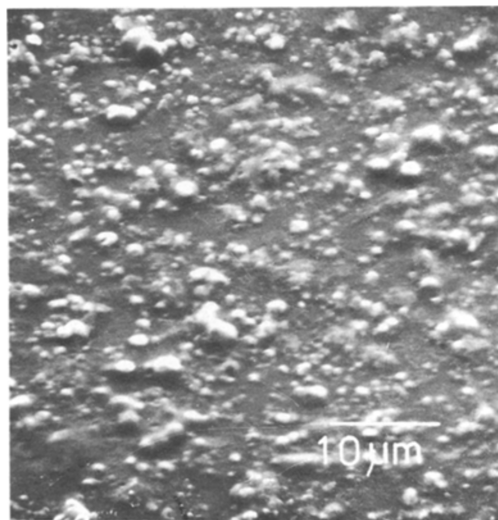

Figure 9 SEM morphology of hot-pressed Si_3N_4 specimen doped with 8 wt% Y_2O_3 + 1 wt% MgO and oxidized at 1193 K for 30 h.

*Hot-pressing conditions: (6.6 wt% CeO_2 + 6.9 wt% SiO_2)–86.5 Si_3N_4, $T = 1923$ K, $P = 29.4$ MPa; 5 wt% CeO_2–95 wt% Si_3N_4, $T = 1923$ K, $P = 29.4$ MPa; (6.9 wt% Y_2O_3 + 5.2 wt% SiO_2)–87.9 Si_3N_4, $T = 1973$ K, $P = 34.3$ MPa; 5 wt% MgO–95 wt% Si_3N_4, $T = 1723$ K, $P = 25.5$ MPa.

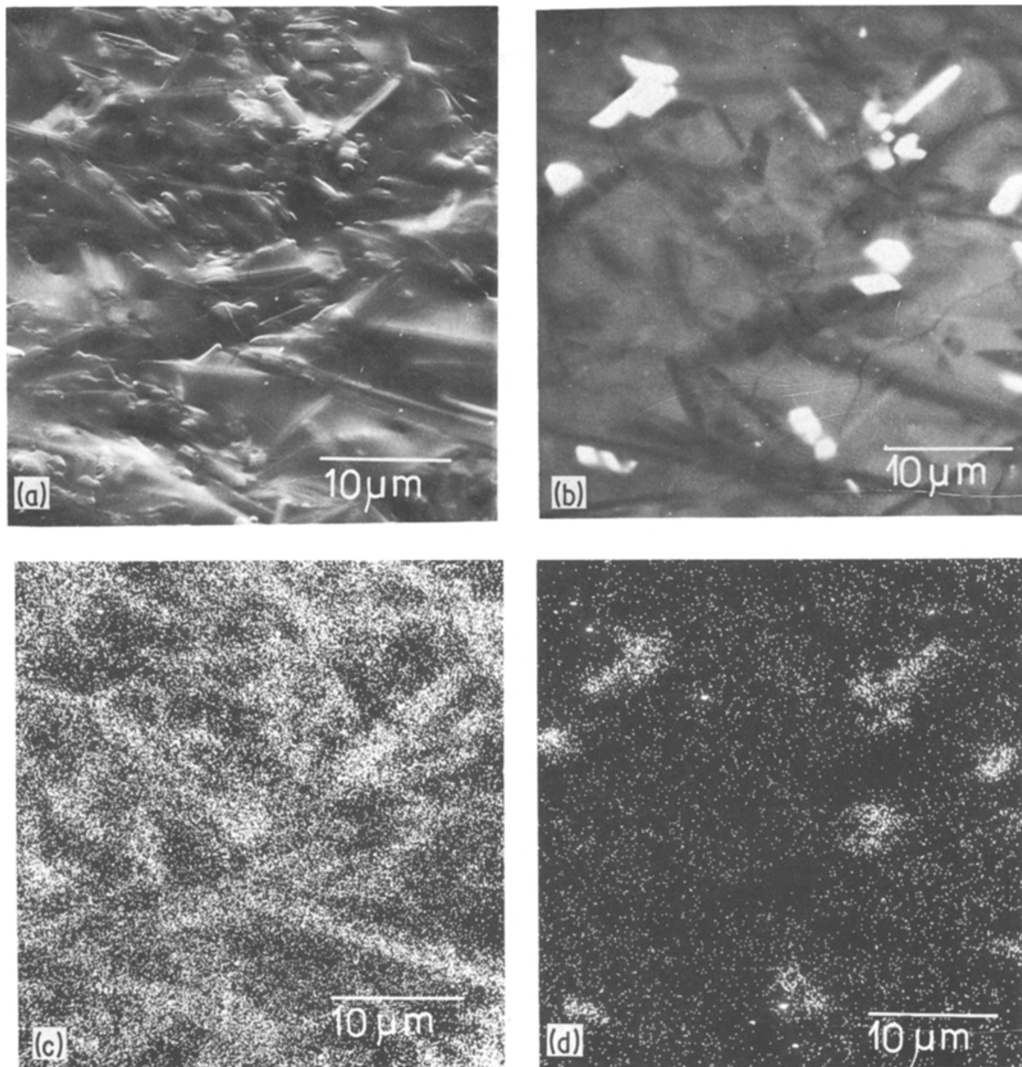

Figure 10 SEM and WDS maps showing concentration of elements on surface of hot-pressed Si_3N_4 specimen doped with 8 wt% Y_2O_3 + 1 wt% MgO and oxidized at 1383 K for 30 h. (a) morphology, (b) back-scattered electron image, (c) Mg, (d) Y.

trations of the intergranular phase, (see Fig. 9), but a very thin amorphous silica film should also form on exposed silicon nitride grains by direct reaction with atmospheric oxygen.

Well-developed cristobalite, akermanite and diopside crystals (dark areas in Fig. 10b), and elongated or isometric $Y_2Si_2O_7$ platelets (white areas in Fig. 10b) contained in an X-ray amorphous silica-phase rich in Mg, Ca and Y, appear to cover almost all the sample surface at 1383 and 1403 K (Figs 10 and 11).

3.2.2. Oxidation at 1440 K $< T <$ 1600 K

Yttrialite and miserite (at $\gtrless$ 1400 K), and the calcium magnesium silicates, akermanite and diopside (at $\gtrless$ 1500 K), decompose. Magnesium silicate ($MgSiO_3$) crystallites, mainly as protoenstatite at ~ 1500 K and mainly as enstatite and clinoenstatite at ~ 1600 K. Two different yttrium silicates of the same unit formula $Y_2Si_2O_7$ but differing in their structure [14, 15] also form. Therefore most of the silica resulting from oxidation is combined in the crystal phase and the relative amount of cristobalite reaches its minimum value (see Fig. 8).

Prismatic $MgSiO_3$ crystals (~ 6 μm x 2 μm in size) and yttrium silicate platelets are clearly observed after oxidation at 1493 K (Fig. 12a and

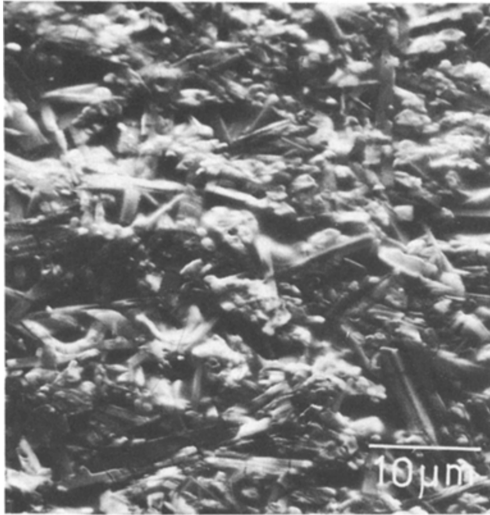

Figure 11 SEM of hot-pressed Si_3N_4 specimen doped with 8 wt% Y_2O_3 + 1 wt% MgO and oxidized at 1403 K for 30 h.

b). The appearance on the oxide scale at 1593 K (Fig. 13a and c) of yttrium silicate dendrites and some incipient rounding-off of the edges of the magnesium silicate (mainly enstatite) crystals, suggest the local occurrence of some liquid phase at the oxidation temperature. The low crystalline silica content at this temperature might also result from the heavy concentration of additive and impurity atoms in the oxide film which form low-melting amorphous silicates.

SEM and WDS studies on the cross-section of the fractured oxide scales of a sample oxidized at 1693 K (Fig. 14a, g) show:

(1) a thin low-melting amorphous surface oxide film 1 to 2 μm thick covering the external oxide surface in which most of the impurity atoms are concentrated;

(2) large $MgSiO_3$ grains covered or partially emerging from the above film;

(3) $Y_2Si_2O_7$ plate-like crystals contained in the interior of the oxide, generally beneath the $MgSiO_3$ grains and never emerging from the outer surface oxide film;

(4) $Y_2Si_2O_7$ dendrides mostly concentrated in the surface oxide film.

Points (1), (3) and (4) confirm the genesis of the two different $Y_2Si_2O_7$ crystal forms, i.e. nucleation and growth at the oxidation temperature for the plate-like morphology and devitrification on cooling for the dendritic one.

3.2.3. Oxidation at $T > 1600$ K

A drastic change in the structure of the oxide film surface occurs at > 1600 K with a relevant increase in the relative amount of crystalline silica (cristobalite + β-quartz) and a decrease of both yttrium and magnesium silicates. Enstatite and/or clinoenstatite crystals, and many $Y_2Si_2O_7$ dendrites are nevertheless present in the oxide scale (Figs 15 and 16). Owing to the very high oxidation rate constants deriving also from softening of the intergranular phase, most of the SiO_2 product from oxidation cannot enter in crystalline or amorphous

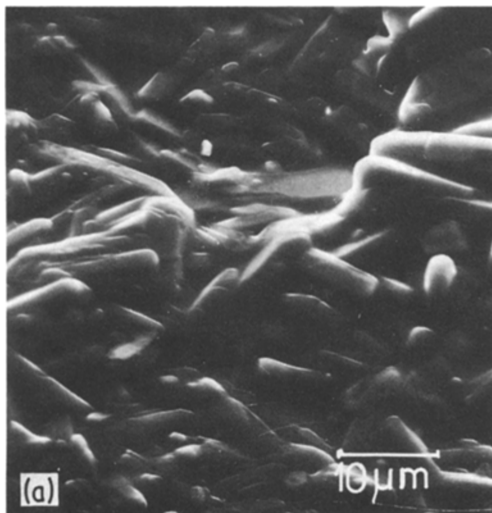

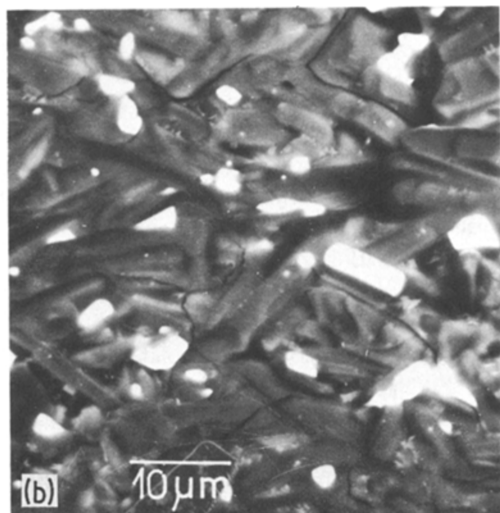

Figure 12 SEMs and WDS maps showing concentration of elements on surface of hot-pressed Si_3N_4 specimen doped with 8 wt% Y_2O_3 + 1 wt% MgO and oxidized at 1493 K for 30 h. (a) morphology, (b) back-scattered electron image.

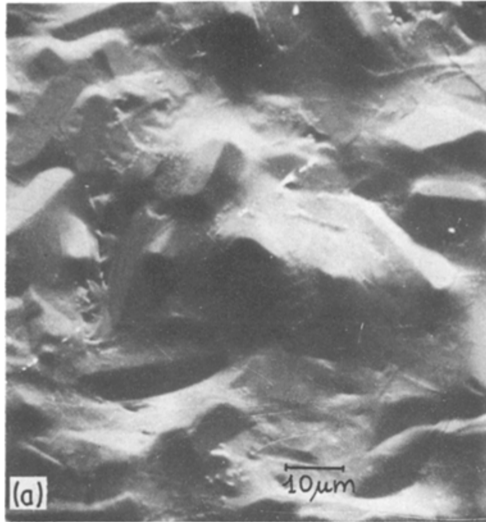

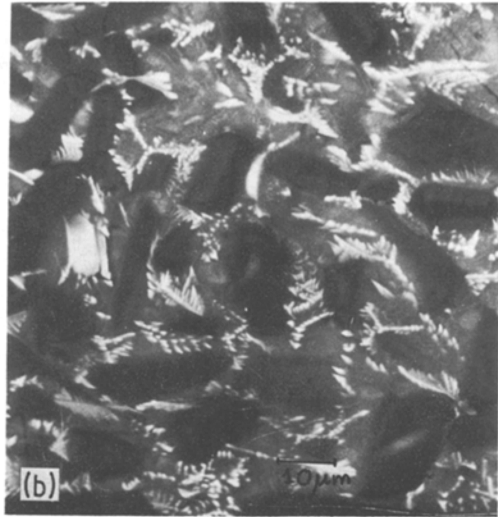

Figure 13 SEMs and WDS map showing concentration of Mg on surface of hot-pressed Si_3N_4 specimen doped with 8 wt% Y_2O_3 + 1 wt% MgO and oxidized at 1593 K for 30 h. (a) morphology (b) back-scattered electron image, (c) Mg map.

silicates. Large elongated β-quartz and granular cristobalite crystals are therefore nucleated and their growth possibly occurs at the oxidation temperature.

Other relevant features which might affect the oxidation behaviour are:

(1) fractures of the oxide scale which can be observed at oxidation temperatures as low as 1400 K and which increase in importance with increasing oxide thickness. These may originate from different sources such as volume changes associated with solid-state crystallization (mainly at lower temperatures) or devitrification phenomena on cooling (especially at high temperature), mismatch among the thermal expansion coefficients of the different phases in the oxide and with the silicon nitride substrate;

(2) the many N_2 escape pores observed on the oxide film surface at oxidation temperatures. At higher oxidation temperatures, owing to the high evolution rate of gaseous nitrogen, larger bubbles are grown some of which are pinned at the nitride/oxide reaction interfaces (see Fig. 17). Other bubbles possibly blow-out any trace being lost on the oxide surface as a consequence of its low viscosity.

4. Discussion

No data are known on the oxidation of HPSN containing both Y_2O_3 and MgO as additives.

Diffusion in the most probable rate-controlling mechanism in oxidation of Y_2O_3-doped HPSN [5, 6]. Cation diffusion through the grain-boundary phase to the nitride/oxide reaction interface, i.e. similar to MgO-doped materials [16, 20], has been recognized as the probable rate-limiting step in short-term oxidation tests (up to ~ 30 h) [5] at 1700 K, the oxide layer appearing somewhat protective for Y_2O_3-doped materials [5] and being absolutely non-protective for MgO-doped materials [21, 22]. At temperatures > 1700 K, it has been suggested that mechanical disruption of the oxide film and the presence of large N_2 bubbles allow gaseous oxygen to flow into the interface between the oxide layer and the unoxidized material thus causing substantial amounts of

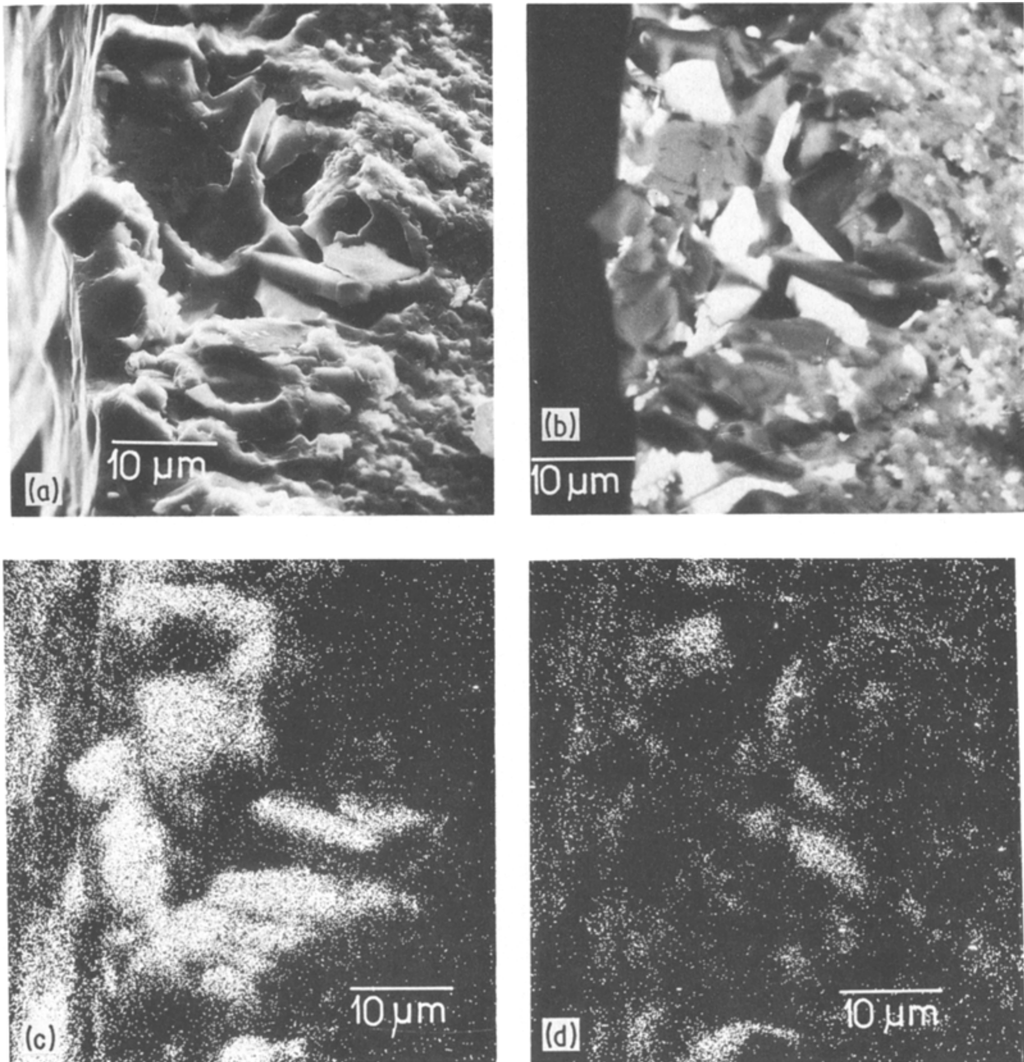

Figure 14 SEMs and WDS maps showing concentration of elements of cross-section of hot-pressed Si_3N_4 specimen doped with 8 wt% Y_2O_3 + 1 wt% MgO and oxidized at 1593 K for 30 h. (a) morphology, (b) back-scattered electron image, (c) Mg, (d) Y, (e) Si, (f) Ca, (g) Al.

fresh surfaces to be exposed to direct reaction with oxygen. Oxygen diffusion through the surface oxide layer has been suggested as the rate-controlling mechanism in long-term oxidation studies above a critical transition temperature (~ 1620 K) [6]. Below this temperature the surface oxide contains a highly connected pore structure, it is non-protective and linear oxidation kinetics were observed [6].

A model for evaluating the oxidation behaviour of HPSN materials based on the classical Fick's diffusion theory [23] was successfully applied to a range of additive systems [24]. This model accounts for the effect on oxidation kinetics of the type and amount of grain-boundary phase and of the composition of the Si_3N_4/oxide reaction interface, and proves useful also for a qualitative description of the experimental behaviour of (Y_2O_3 + MgO)-doped HPSN, its most striking feature being represented by the three apparently different oxidation regimes in different temperature regions.

The first oxidation regime extends in the thermal stability field of yttrialite and miserite. These phases take in solid solution part of the additive and impurities, thus hindering their diffusion. A direct silicon nitride/oxygen interaction [$(Si_3N_4 + 3O_2) \rightarrow 3\,SiO_2 + 2\,N_2\uparrow$], with oxygen diffusion

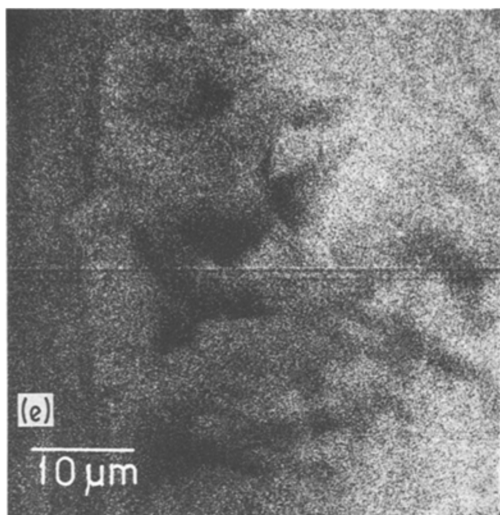

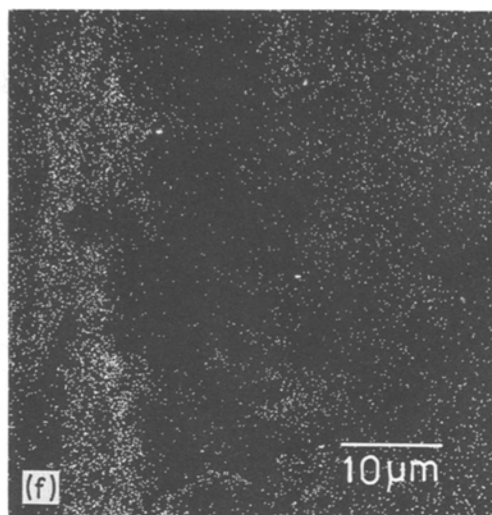

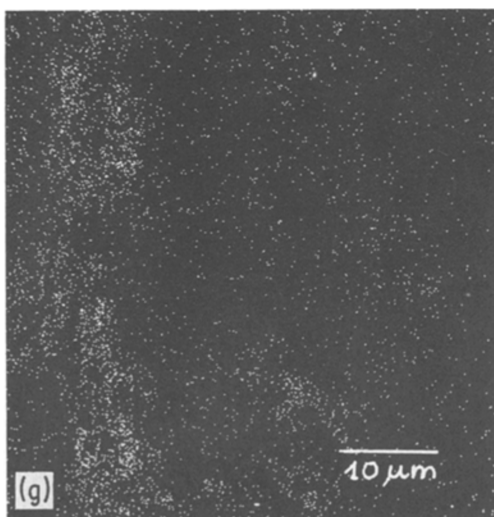

Figure 14 Continued.

through the thin oxide layer as the controlling step, might be envisaged in this stage to account for the low apparent activation energy for oxidation $\Delta H = 120\,\text{kJ mol}^{-1}$. Results of studies on oxygen transport through the pure SiO_2-layers parabolically grown during the oxidation of elemental silicon [25] and pure silicon compounds such as SiC [25] and $MoSi_2$ [26], for which permeation of molecular oxygen through the SiO_2 [27] is suggested as the controlling step give, in fact, values for ΔH of 126 to 167 kJ mol^{-1}.

For oxidation of pure silicon nitride powders [28] a higher ΔH value is obtained at $T < 1473$ K, this being possibly related to the drastic decrease in oxygen mobility below the glass transition temperature [29, 30] which is about 1473 K for vitreous silica but which can be greatly lowered in our case by the presence of the metallic ions diffusing from the grain-boundary phase to the SiO_2 layer.

The second temperature regime ($1400 < T < 1600$ K) is one in which the dominant oxidation mechanism is the diffusion of additive and impurities through the highly viscous grain-boundary phase to the silicon nitride/oxide reaction interface. The corresponding value of $580\,\text{kJ mol}^{-1}$ for the apparent activation energy for oxidation is somewhat higher than for materials obtained by using Y_2O_3 additive [5], this being possibly related to the different properties of the intergranular phase which are affected by the presence of MgO. Owing to dissolution of yttrialite and miserite solid solutions, all additive and impurity cations are allowed to diffuse freely. This accounts for the variation in composition of the oxide film which enriches in Ca–Mg silicates.

Lower activation energies have been reported at homologous temperatures for MgO- [16] (433 kJ mol^{-1}), CeO_2- [31] (385 to $400\,\text{kJ mol}^{-1}$) and ($CeO_2 + SiO_2$)-doped [32] ($350\,\text{kJ mol}^{-1}$) HPSN, whereas activation energies ranging from 200 to $620\,\text{kJ mol}^{-1}$ pertain to materials hot pressed from the Si_3N_4–Y_2O_3–SiO_2 system [23].

In the third oxidation regime, the diffusion of cations also in the integranular phase remains the rate-governing step for oxidation, a synergetic effect being represented by the softening of the grain-boundary phase. Very high oxidation rates

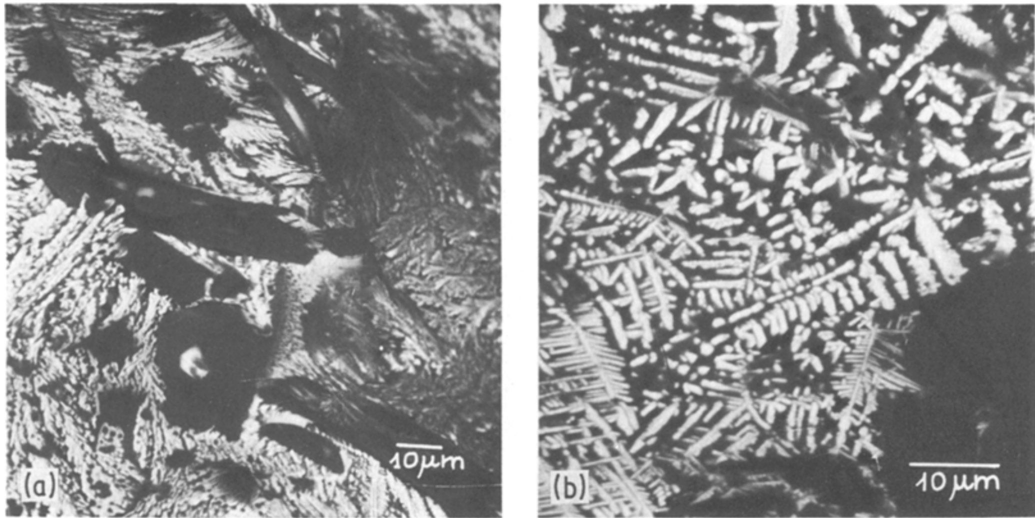

Figure 15 SEMs of surface of hot-pressed Si_3N_4 specimen doped with 8 wt % Y_2O_3 + 1 wt % MgO and oxidized at 1653 K for 30 h. (a) and (b) back-scattered electron images.

result from the enhanced diffusion. The ΔH value of $\sim 960\,kJ\,mol^{-1}$ is similar to that of 980 kJ mol^{-1} reported [5] for Y_2O_3-doped HPSN at $T > 1730\,K$, which was claimed [5] to derive from mechanical disruption of the oxide film.

5. Conclusions

After an initial transient stage in which direct reaction with atmospheric oxygen might be suggested to govern oxidation, diffusion of additive and impurity species to the silicon nitride/oxygen interface appears the most likely rate-governing mechanism in the oxidation of (Y_2O_3 + MgO)-doped HPSN.

The oxidation resistance of this material at low temperature appears somewhat better than for MgO-doped HPSN and approaches that of Y_2O_3-doped HPSN. At higher temperatures, i.e., above the stability field of miserite and yttrialite, the oxidation rates become comparable to MgO-doped HPSN.

The presence of crystalline compounds in the grain-boundary phase which are able to accommodate in their structure additive and impurity

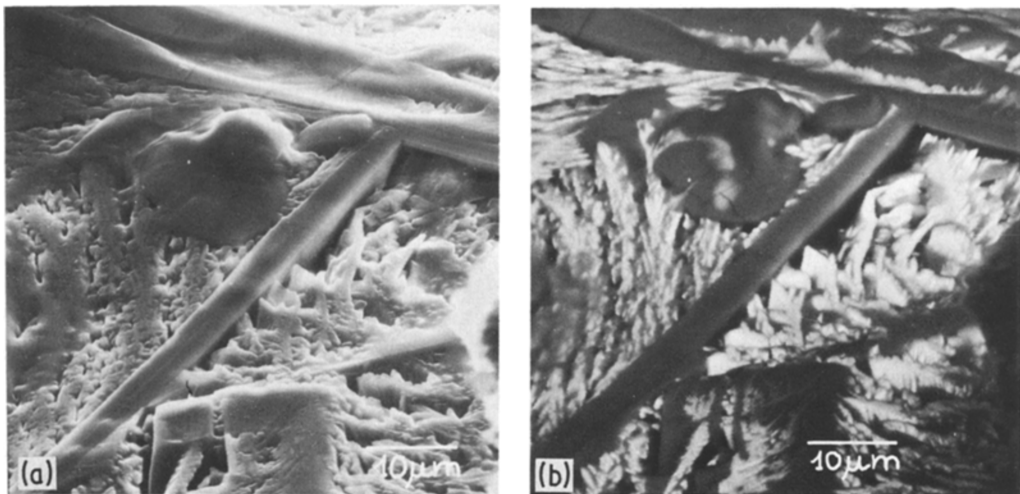

Figure 16 SEMs and WDS maps showing concentration of elements on surface of hot-pressed Si_3N_4 specimen doped with 8 wt % Y_2O_3 + 1 wt % MgO and oxidized at 1653 K for 30 h. (a) Morphology, (b) back-scattered electron image, (c) Si, (d) Mg, (e) Y.

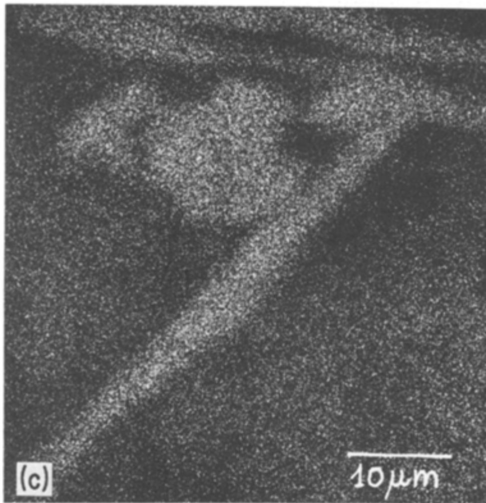

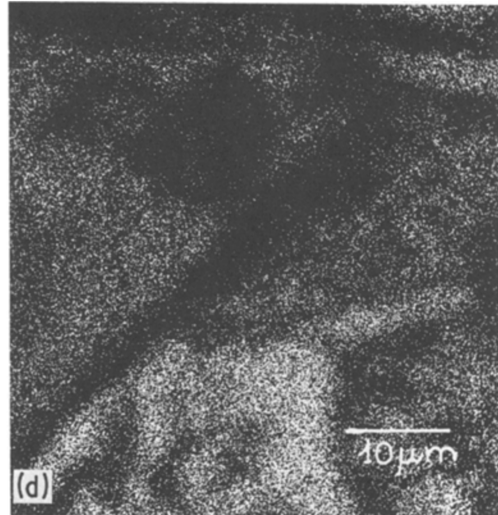

Figure 16 Continued.

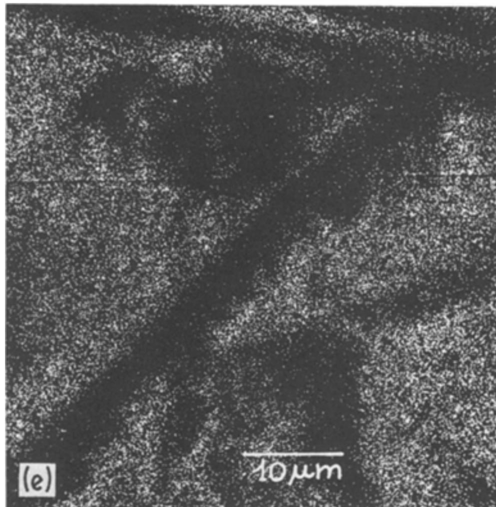

cations, is therefore suggested as a suitable way of improving the oxidation resistance of hot-pressed or pressureless-sintered silicon nitride in a temperature range in which the above phases are stable.

References

1. F. F. LANGE, S. C. SINGHAL and R. C. KUZNICKI, *J. Amer. Ceram. Soc.* 60 (1977) 249.
2. L. J. GAUKLER, H. HOHNKE and T. Y. TIEN, *ibid.* 63 (1980) 35.
3. R. R. WILLS, J. A. CUNNINGHAM, J. M. WIMMER and R. W. STEWART, *ibid.* 59 (1976) 269.
4. G. Q. WEAVER and J. W. LUCEK, *Amer. Ceram. Soc. Bull.* 57 (1978) 1131.
5. D. CUBICCIOTTI and K. H. LAU, *J. Electrochem. Soc.* 126 (1979) 1723.
6. C. L. QUACKENBUSH and J. T. SMITH, *Amer. Ceram. Soc. Bull.* 59 (1980) 533.
7. Y. HASEGAWA, H. TANAKA, M. TSUTSUMI and H. SUZUKI, *Yogyo-Kyokai-Shi* 88 (1980) 292.
8. A. GIACHELLO, P. C. MARTINENGO, G. TOMMASINI and P. POPPER, *Amer. Ceram. Soc. Bull.* 59 (1980) 1212.
9. J.C.P.D.S. (International Center for Diffraction Data) Powder diffraction file 22-806.
10. J.C.P.D.S. (International Center for Diffraction Data) Powder diffraction file 21-1459.
11. J.C.P.D.S. (International Center for Diffraction Data) Powder diffraction file 21-1457.
12. J.C.P.D.S. (International Center for Diffraction Data) Powder diffraction file 21-1460.
13. J.C.P.D.S. (International Center for Diffraction Data) Powder diffraction file 22-1004.

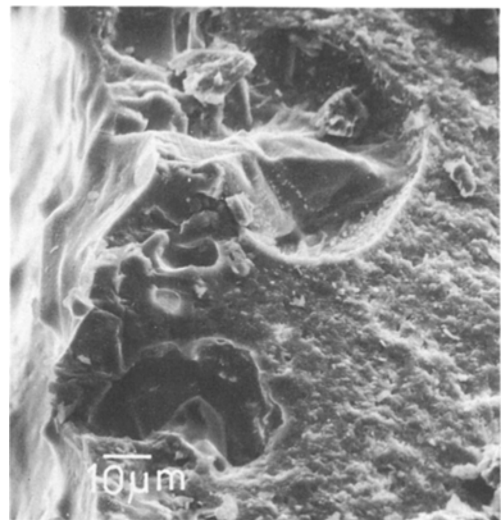

Figure 17 SEMs of cross-section of hot-pressed Si_3N_4 specimen doped with 8 wt% Y_2O_3 + 1 wt% MgO and oxidized at 1593 K for 30 h: morphology.

14. J.C.P.D.S. (International Center for Diffraction Data) Powder diffraction file 22-1103.
15. J.C.P.D.S. (International Center for Diffraction Data) Powder diffraction file 20-1416.
16. G. N. BABINI, A. BELLOSI and P. VINCENZINI, *Ceramica* 3 (1981) 11.
17. S. C. SINGHAL, *J. Mater. Sci.* **11** (1976) 500.
18. D. C. CUBICCIOTTI and K. H. LAU, *J. Amer. Ceram. Soc.* **61** (1978) 512.
19. A. J. KIEHLE, L. K. HEUNG, P. J. GIELISSE and T. J. ROCKETT, *ibid.* **58** (1975) 17.
20. W. C. TRIPP and H. C. GRAHAN, *J. Amer. Ceram. Soc.* **59** (1976) 399.
21. D. CUBICCIOTTI, K. H. LAU and R. L. JONES, *J. Electrochem. Soc.* **124** (1977) 1955.
22. D. CUBICCIOTTI and K. H. LAU, *ibid.* **61** (1979) 512.
23. G. N. BABINI, A. BELLOSI and P. VINCENZINI, "Oxidation kinetics of silicon nitride hot-pressed with Yttria and Silica additions", paper presented at the 83rd Annual Meeting of the American Ceramic Society, Washington, April 1981 (Abstract in *Amer. Ceram. Soc. Bull.* **60** (1981) 379).
24. G. N. BABINI and P. VINCENZINI, "Oxidation kinetics of hot pressed silicon nitride" paper presented at the 2nd NATO/ASI "Nitrogen Ceramics", Falmer, Brighton, UK. August 1981 in press.
25. K. MOTZFELD, *Acta Chem. Scand.* **18** (1956) 1596.
26. E. FITZER and K. REINMUTH, in "Hochtemperaturwerkstoffe", 6 Plansee Seminar, edited by F. Benesovsky, June 1968, Reutte (Springer Verlag, Wein, 1969) pp. 767.
27. F. J. NORTON, *Nature (London)* **191** (1951) 859.
28. E. FITZER and R. EBI, in "Silicon Carbide 1973", edited by R. C. Marshall, J. W. Faust, C. E. Ryan (University of South Carolina Press, Columbia, South Carolina, 1974) p. 320.
29. K. MUEHLENBACHS and H. A. SCHAEFFER, *Canad. Mineral.* **15** (1977) 179.
30. T. B. KING and P. J. KOROS, in "Kinetics of High Temperature Processes", edited by W. D. Kingery (M.I.T. Technology Press, Cambridge, Mass., 1959) p. 80.
31. G. N. BABINI, A. BELLOSI and P. VINCENZINI, *J. Amer. Ceram. Soc.* **64** (1981) 578.
32. *Idem, Ceram. Int.* 7 (1981) 78.

Received 8 March
and accepted 2 July 1982